www.acsnano.org

# Interlayer Incorporation of A-Elements into MXenes Via Selective Etching of A' from $M_{n+1}A'_{1-x}A''_{x}C_{n}$ MAX Phases

Saman Bagheri, Alexey Lipatov, Nataliia S. Vorobeva, and Alexander Sinitskii\*



Downloaded via UNIV OF NEBRASKA LINCOLN on March 20, 2024 at 21:32:06 (UTC). See https://pubs.acs.org/sharingguidelines for options on how to legitimately share published articles.

Cite This: ACS Nano 2023, 17, 18747-18757



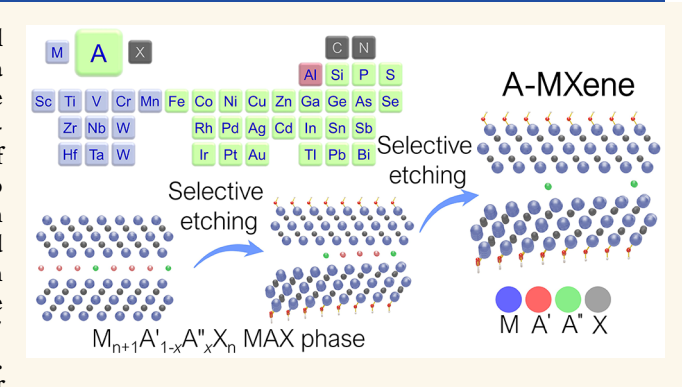
**ACCESS** 

III Metrics & More

Article Recommendations

s Supporting Information

**ABSTRACT:** MXenes are a large family of two-dimensional materials with a general formula  $M_{n+1}X_nT_z$ , where M is a transition metal, X = C and/or N, and  $T_z$  represents surface functional groups. MXenes are synthesized by etching A-elements from layered MAX phases with a composition of  $M_{n+1}AX_n$ . As over 20 different chemical elements were shown to form A-layers in various MAX phases, we propose that they can provide an abundant source of very diverse MXene-based materials. The general strategy for A-modified MXenes relies on the synthesis of  $M_{n+1}A'_{1-x}A''_xX_n$  MAX phase, in which the higher reactivity of the A'-element compared to that of A'' enables its selective etching, resulting in A''-modified  $M_{n+1}X_nT_z$ . In general, the A''-element could modify the interlayer spaces of



MXene flakes in a form of metallic or oxide species, depending on its chemical identity and synthetic conditions. We demonstrate this strategy by synthesizing Sn-modified  $Ti_3C_2T_z$  MXene from the  $Ti_3Al_{0.75}Sn_{0.25}C_2$  MAX phase, which was used as a model system. Although the incorporation of Sn in the A-layer of  $Ti_3AlC_2$  decreases the MAX phase reactivity, we developed an etching procedure to completely remove Al and produce Sn-modified  $Ti_3C_2T_z$  MXene. The resulting MXene sheets were of very high quality and exhibited improved environmental stability, which we attribute to the effect of a uniform Sn modification. Finally, we demonstrate a peculiar electrostatic expansion of Sn-modified  $Ti_3C_2T_z$  accordions, which may find interesting applications in MXene-based nano-electromechanical systems. Overall, these results demonstrate that in addition to different combinations of M and X elements in MAX phases, an A-layer also provides opportunities for the synthesis of MXene-based materials.

**KEYWORDS:** MXene, MAX phase,  $Ti_3C_2T_2$ , tin, selective etching, environmental stability, nano-electromechanical systems

# INTRODUCTION

MXenes are a large family of two-dimensional transition-metal carbides, nitrides, and carbonitrides with diverse physical properties and applications.  $^{1,2}$  The general chemical formula of MXenes is  $M_{n+1}X_nT_z$ , where M is a transition metal, such as Ti, Cr, Nb, Ta, etc., X is carbon and/or nitrogen, n=1,2,3,4, and 5, and  $T_z$  represents surface functional groups. MXenes are synthesized by selective etching of the A-element from layered MAX phases, with a general formula of  $M_{n+1}AX_n$ , in which the A-layers separate the  $M_{n+1}X_n$  layers. Although elements such as Fe, Ir, Cu, Au, Ga, Sb, Si, etc., from Groups 8 through 16 can be used as components of the A-layers,  $^{3,4}$  the most frequently used A-element is aluminum, with the most established etching process.  $^{5,6}$ 

Despite ongoing investigations on numerous combinations of M and X elements, such as  ${\rm Ti}_3{\rm C}_2$ ,  ${}^{5,7}$   ${\rm Ti}_2{\rm C}$ ,  ${}^8$   ${\rm Ti}_2{\rm N}$ ,  ${}^9$   ${\rm Ti}_3{\rm CN}$ ,  ${}^{10}$   ${\rm Nb}_2{\rm C}$ ,  ${}^{11}$   ${\rm Nb}_4{\rm C}_3$ ,  ${}^{12,13}$   ${\rm V}_2{\rm C}$ ,  ${}^{14,15}$   ${\rm Cr}_2{\rm Ti}{\rm C}_2$ ,  ${}^{16}$   ${\rm Mo}_4{\rm VC}_4$ ,  ${}^{17}$  TiVNb-

MoC<sub>3</sub>, and TiVCrMoC<sub>3</sub>, <sup>18</sup> and their impact on MXene synthesis, product quality, and characteristics, there has been far less interest in exploring the chemical diversity and significance of the A-element for the synthesis of MXene materials. <sup>19,20</sup> Yet, the known MAX phases contain a large variety of elements in their A-layers (Figure 1a), either as single elements or as combinations of different elements, potentially providing plentiful opportunities for the synthesis of MXene-based materials.

Received: March 8, 2023
Accepted: July 27, 2023
Published: September 25, 2023





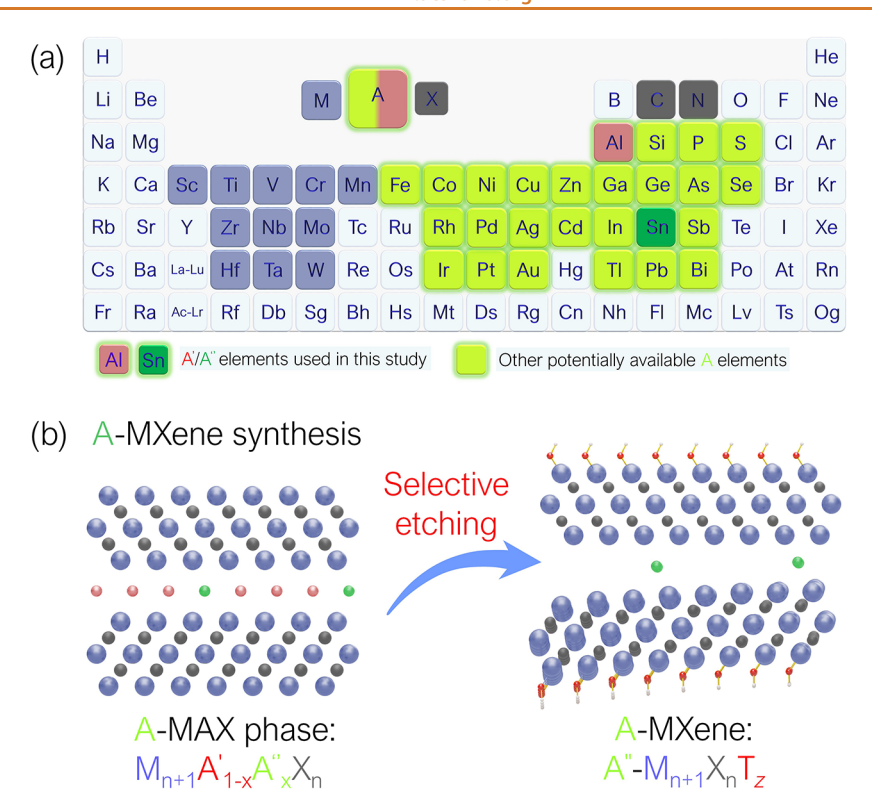


Figure 1. Schematic illustration of the proposed synthetic approach. (a) Periodic Table of MAX phases. The data were collected from review papers on MAX phases,  $^{3,4}$  as well as recent literature. Blue represents transition metals for the M layer, black represents the X elements, and green and red represent the available elements for the A-layer (Al is shown in red as the most frequently used A-element for the MXene synthesis, and Sn is shown in dark green as the second A-element used in this study). (b) Scheme of the selective etching of the A'-element from the  $M_{n+1}A'_{1-x}A''_{x}X_{n}$  MAX phase to form  $A''-M_{n+1}X_{n}T_{z}$  MXene. The functional groups between the split  $M_{n+1}X_{n}$  layers are omitted for clarity.

While the A-element is not directly included in the MXene layers, the plethora of MAX phases with a great chemical diversity of A-layers could be a rich source of MXene-based materials and composites. Many studies involve various MXenes in combination with other functional materials, such as metals, oxides, etc. 21-38 A general synthetic approach for such composite materials is to first synthesize a MXene by completely removing the A-element from the precursor MAX phase and then modify it with another material of interest. One recently developed approach focusing on the chemistry of Aelements involves Lewis acidic molten salts (LAMS) and LAMS scissors, 39,40 enabling a control over the A-layer elements and their substitution using strategically designed etching methods. In this work, we suggest a different approach by which the A-elements can be integrated with MXenes directly at the MXene synthesis step without a need for any postprocessing.

In order to implement this approach, we suggest the following synthetic strategy. If there is a need to synthesize a MXene material modified with an element A'', one should select a complementary A-layer element, which we label as A', that could form  $M_{n+1}A'_{1-x}A''_{x}X_{n}$  MAX phase and would be easier to etch than the A''-element. Then, if a pair of A' and A'' elements is properly chosen, it would be possible to utilize the difference in their reactivities to selectively etch away the A' while leaving the A'' between the MXene layers, as shown in Figure 1b. The resulting material could be described as A-MXene, suggesting that MXene is still formed from the corresponding MAX phase precursor but the A-element is not

eliminated entirely and modifies the interlayer spaces of the flakes.

This approach is expected to have multiple advantages for advancing the field of MXene materials. First, it potentially provides access to many possible combinations of different A"elements and different MXenes, and such complex materials could be synthesized in a single step by etching the corresponding MAX phases. Furthermore, instead of a single A"-element, several such elements could be potentially incorporated in the A-layer of a precursor MAX phase and combined with a sacrificial A'-element with higher reactivity. Second, the x content of the A"-element could be controlled during the synthesis of the  $M_{n+1}A'_{1-x}A''_{x}X_{n}$  MAX phase. Third, the A"-element distribution within the A-layers of the precursor MAX phase is very uniform and is expected to translate into the uniform modification of the resulting MXenes. This is an important advantage over postsynthesis modifications of MXenes, such as atomic layer deposition (ALD),<sup>29</sup> in situ growth of metal oxide nanoparticles,<sup>36</sup> etc., that often result in nonuniform nucleation of nanoparticles at the edges and defect sites of the flakes.

The A-elements shown in Figure 1a are found in various metallic and oxide materials that are known for a great variety of very diverse functional properties, and the combinations of these materials with MXenes are expected to find applications in catalysis, energy storage, gas sensing, and other fields. Examples of such MXene-nanoparticle composites are very abundant. For instance, CuO and ZnO are among very common metal oxides that were, either physically or chemically, incorporated into  $\mathrm{Ti}_3\mathrm{C}_2\mathrm{T}_z$  for applications in the

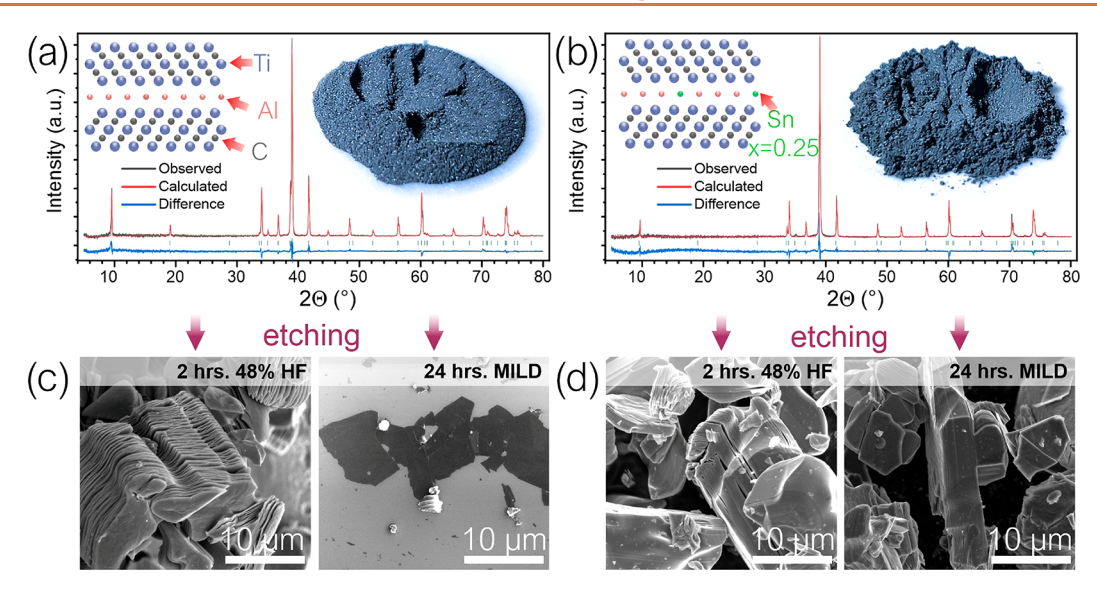


Figure 2. Comparison of etching behavior of  $Ti_3AlC_2$  and  $Ti_3AlC_2$ 5  $Sn_{0.25}C_2$  MAX phases. (a, b) XRD patterns of (a)  $Ti_3AlC_2$  and (b)  $Ti_3Al_{0.75}Sn_{0.25}C_2$  MAX phase powders with their Rietveld refinement. The experimental data are shown in black, theoretical fits are shown in red, the differences are shown in blue, and the green vertical bars indicate the Bragg angles. The insets show structures of the  $Ti_3AlC_2$  and  $Ti_3Al_{0.75}Sn_{0.25}C_2$  MAX phases as well as optical photographs of their powders. (c) Representative SEM images of the etching products obtained from the  $Ti_3AlC_2$  MAX phase by 2 h treatment with 48% HF (left) and 24 h etching using the MILD method (right). (d) Representative SEM images of the etching products obtained from the  $Ti_3Al_{0.75}Sn_{0.25}C_2$  MAX phase by 2 h treatment with 48% HF (left) and 24 h etching using the MILD method (right).

detection of organic vapors,<sup>21</sup> hydrogen evolution reaction (HER),<sup>22</sup> photo-electrochemical water splitting,<sup>23</sup> and many other areas.<sup>24–28</sup> Among other nanoparticles, Pt, Pd, Sn, Ag, SnS<sub>2</sub>, Fe<sub>3</sub>O<sub>4</sub>, and SnO<sub>x</sub> have been extensively combined with MXenes for applications in batteries,<sup>29,30</sup> gas sensors,<sup>32,33</sup> solar cells,<sup>34</sup> ion storage,<sup>35,36</sup> and supercapacitors.<sup>37</sup> All of these metallic elements are known to be components of A-layers in various MAX phases (Figure 1a), which means that their integration with MXenes may be possible through the suggested synthetic approach (Figure 1b).

Considering the multitude of these synthetic and application opportunities, we could not explore all of them in this study and focused on a single model MXene material as a proof of concept. We demonstrate the viability of the described synthetic strategy (Figure 1b) by considering Al as A'-element and Sn as A"-element and preparing a Sn-modified Ti<sub>3</sub>C<sub>2</sub>T<sub>z</sub> MXene. The choice of this model material was supported by the availability of both Ti<sub>3</sub>AlC<sub>2</sub> and Ti<sub>3</sub>SnC<sub>2</sub> MAX phases as well as differences in their etching behavior. Ti<sub>3</sub>AlC<sub>2</sub> is the most common precursor in MXene synthesis, while Ti<sub>3</sub>SnC<sub>2</sub> is not etchable using the standard procedures established for Al removal from Ti<sub>3</sub>AlC<sub>2</sub>, which we verified in our preliminary studies.

We synthesized the  $Ti_3AI_{0.75}Sn_{0.25}C_2$  MAX phase and used it as a precursor for  $Sn-Ti_3C_2T_z$  MXene according to the general procedure shown in Figure 1b. We found that while the incorporation of Sn in the A-layer of the MAX phase decreases its etching reactivity, with a modified etching procedure discussed in this work, it is possible to completely remove Al and produce  $Ti_3C_2T_z$  MXene uniformly modified with tin. Despite the use of harsher conditions than those needed for the etching of  $Ti_3AlC_2$ , the resulting MXene sheets were of very high quality and exhibited improved environmental stability, which we attribute to the effect of Sn modification. Finally, we demonstrate a peculiar electrostatic expansion of the  $Sn-Ti_3C_2T_z$  accordions, which may find interesting

applications in MXene-based nano-electromechanical systems (NEMS). Although we demonstrated the feasibility of the described synthetic approach (Figure 1b) using  $Ti_3Al_{0.75}Sn_{0.25}C_2$  as a model system, the generality of this method should be further investigated in the future with other interesting combinations of A-elements that may potentially include Ir, Cu, Ni, etc. Overall, these results demonstrate that in addition to different combinations of M and X elements in MAX phases, an A-layer also provides opportunities for the synthesis of MXene materials.

# **RESULTS AND DISCUSSIONS**

We compared the etching behavior of Ti<sub>3</sub>Al<sub>0.75</sub>Sn<sub>0.25</sub>C<sub>2</sub> with Ti<sub>3</sub>AlC<sub>2</sub>, which is by far the most studied MAX phase in MXene research<sup>1,2</sup> and thus served as a reference. Both Ti<sub>3</sub>AlC<sub>2</sub> and Ti<sub>3</sub>Al<sub>0.75</sub>Sn<sub>0.25</sub>C<sub>2</sub> were prepared via a hightemperature solid-state synthesis, as described in the Experimental section. The Ti<sub>3</sub>AlC<sub>2</sub> MAX phase was synthesized by annealing a mixture of TiC, Ti, and Al powders under the flow of Ar at 1450 °C. The Sn-modified Ti<sub>3</sub>AlC<sub>2</sub> MAX phase was synthesized using the same procedure but with an addition of Sn to the precursor mixture, as described in the Experimental section. The Ti<sub>3</sub>AlC<sub>2</sub> and Ti<sub>3</sub>Al<sub>0.75</sub>Sn<sub>0.25</sub>C<sub>2</sub> MAX phase samples are visually indistinguishable, appearing as gray powders with a bluish tint; see the optical photographs in Figure 2a,b. The elemental composition of the samples was studied using energy-dispersive X-ray (EDX) spectroscopy. The EDX analysis of the Ti<sub>3</sub>AlC<sub>2</sub> MAX phase confirmed the Ti/Al atomic ratio of 3.0:1.0. In the case of the Sn-modified Ti<sub>3</sub>AlC<sub>2</sub> MAX phase, the EDX analysis showed a Ti/Al/Sn atomic ratio of 3.00:0.77:0.23, which is very close to the expected value based on the precursor mixture composition.

EDX analysis does not provide information about how the tin is incorporated into the structure of the MAX phase. In order to address this question, we employed the Rietveld analysis to find which atomic positions are occupied by Sn

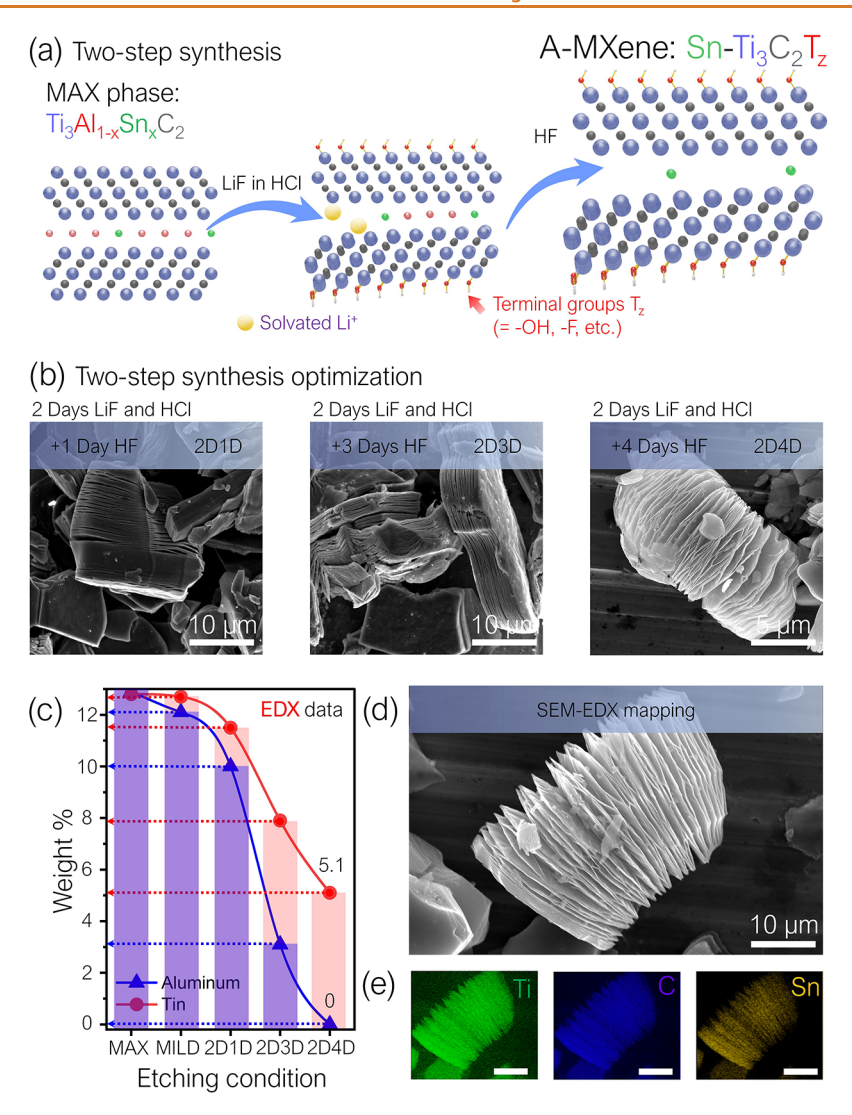


Figure 3. Synthesis of  $Sn-Ti_3C_2T_z$  MXene from  $Ti_3Al_{0.75}Sn_{0.25}C_2$  MAX phase. (a) Scheme of the two-step etching approach; see text for details. The functional groups between the split  $Ti_3C_2$  layers are omitted for clarity. (b) SEM images demonstrating the progression of the etching of  $Ti_3Al_{0.75}Sn_{0.25}C_2$  MAX phase particles with 48% HF after their initial etching for 2 days using the LiF and HCl. (c) The concentrations of Al and Sn in the etching products according to the EDX results. The data are shown in wt % relative to the metal content (Ti, Al, Sn) in  $Ti_3Al_{0.75}Sn_{0.25}C_2$  MAX phase and the etching products due to the limitations of EDX to accurately determine concentrations of light elements (carbon,  $T_z$  functional groups). (d) SEM image of a  $Sn-Ti_3C_2T_z$  MXene accordion produced using the 2D4D method. (e) EDX maps of the  $Sn-Ti_3C_2T_z$  MXene accordion shown in panel (d) for Ti,  $C_z$ , and Sn.

atoms in the crystal structure of Ti<sub>3</sub>AlC<sub>2</sub>. The Rietveld method relies on a careful collection of powder X-ray diffraction (XRD) patterns. Figure 2a,b shows XRD patterns and their Rietveld refinements for both MAX phases, demonstrating that the synthesized Ti<sub>3</sub>AlC<sub>2</sub> and Sn-modified Ti<sub>3</sub>AlC<sub>2</sub> MAX phases were phase-pure and highly crystalline. The general forms of both XRD patterns are very similar, each containing all major peaks that are usually used to identify Ti<sub>3</sub>AlC<sub>2</sub>. However, there are several minor differences in the relative intensities of some peaks, such as the (002) peak at  $2\Theta = 9.5^{\circ}$ , or the visual absence of others, such as the (004) peak at  $2\Theta = 19.5^{\circ}$  and the (008) peak at  $2\Theta = 36.7^{\circ}$  in the Sn-modified MAX phase. The origin of these differences is the presence of foreign atoms in the crystal structure of Ti<sub>3</sub>AlC<sub>2</sub>, which alter the electronic density of the crystallographic planes. The Rietveld method can be used to confirm the crystal structure and get information about the occupation of atomic positions, providing information about the chemical composition of an

analyzed compound. Satisfactory results of the Rietveld refinement for the Sn-modified Ti<sub>3</sub>AlC<sub>2</sub> MAX phase XRD pattern were achieved when 24.24(1)% of Al atomic positions in the A-layer were occupied with Sn, resulting in the composition of Ti<sub>3</sub>Al<sub>0.76</sub>Sn<sub>0.24</sub>C<sub>2</sub>. The unit cell parameters of the  $Ti_3AlC_2$  phase were found to be a = b = 0.30733(1) nm, c= 1.8596(1) nm, and V = 0.15210(1) nm<sup>3</sup>, in line with the previous studies.44 The unit cell parameters of the Ti<sub>3</sub>Al<sub>0.76</sub>Sn<sub>0.24</sub>C<sub>2</sub> MAX phase were found to be almost the same: a = b = 0.30821(1) nm, c = 1.8571(1) nm, and V =0.15277(1) nm<sup>3</sup>. The lack of difference in the unit cell parameters and volume may be surprising, given that the atomic radius of Sn (145 pm) is substantially larger than that of Al (125 pm) and more comparable to Ti (140 pm). However, interatomic distances between Al and Ti of 288 pm in the Ti<sub>3</sub>AlC<sub>2</sub> structure are much larger than the sum of atomic radii of Al and Ti (125 + 140 = 265 pm), meaning that Al is fairly loose inside the trigonal prism formed by six

titanium atoms, and there is room for a larger atom. Indeed, if Al is replaced by Sn, the latter perfectly fits within the structure, as the sum of atomic radii of Sn and Ti (145 + 140 = 285 pm) matches their interatomic distance in the  $Ti_3Al_{0.75}Sn_{0.25}C_2$  structure.

In previous studies, the synthetic approaches for etching Al from Ti<sub>3</sub>AlC<sub>2</sub> were thoroughly investigated and optimized.<sup>6</sup> Historically, concentrated HF was initially employed as an etchant,<sup>5</sup> while later studies shifted toward the LiF-HCl etchant, which is used in the well-established minimally intensive layer delamination (MILD) method.<sup>45</sup> Another important attribute of the MILD method is the avoidance of any ultrasonication of the reaction mixture and the etching products to preserve the flake size of Ti<sub>3</sub>C<sub>2</sub>T<sub>z</sub> MXene. 46,47 We compared the efficiencies of the 48% HF and MILD methods for etching the A-elements from the Ti<sub>3</sub>Al<sub>0.75</sub>Sn<sub>0.25</sub>C<sub>2</sub> and Ti<sub>3</sub>AlC<sub>2</sub> MAX phases. The scanning electron microscopy (SEM) images demonstrating the results of these etching experiments are shown in Figure 2c,d. The etching of Ti<sub>3</sub>AlC<sub>2</sub> with 48% HF for 2 h successfully removes Al layers from bulk MAX phase particles, splitting them into  $Ti_3C_2T_z$  MXene accordions, as shown in the left panel in Figure 2c. The use of a LiF-HCl mixture for 24 h is also very efficient for etching Ti<sub>3</sub>AlC<sub>2</sub>. The MILD delamination protocol that avoids ultrasonication results in the solution exfoliation of the MXene accordions into large individual Ti<sub>3</sub>C<sub>2</sub>T<sub>z</sub> flakes; see the right panel in Figure 2c. With proper optimization of the delamination procedure, these flakes can be made into monolayers and reach tens of micrometers in lateral size. 46,47

Figure 2d shows SEM images of the products of the initial attempts to etch Ti<sub>3</sub>Al<sub>0.75</sub>Sn<sub>0.25</sub>C<sub>2</sub> by using the same protocols. For the Sn-modified MAX phase, we did not observe the formation of separate layers using either method. The 24 h MILD method left Ti<sub>3</sub>Al<sub>0.75</sub>Sn<sub>0.25</sub>C<sub>2</sub> particles almost intact, as shown in the right panel in Figure 2d. The 2 h etching with 48% HF was slightly more aggressive and resulted in some particle grains being etched in the center, as seen in the left panel in Figure 2d. These results show that substitution of even 25% of Al atoms with Sn in Ti<sub>3</sub>AlC<sub>2</sub> dramatically changes the etching behavior of the resulting MAX phase, decreasing its chemical reactivity. Interestingly, a recent theoretical study investigated the synthesizability of MXenes from various MAX phases, including Ti<sub>3</sub>AlC<sub>2</sub> and Ti<sub>3</sub>SnC<sub>2</sub>. 48 Overall, from 1122 MAX phase candidates, only 466 MAX phases were predicted to be synthesizable, and 136 MAX phases were predicted to be etchable to make 26 MXenes. 48 In the case of the Ti<sub>3</sub>AlC<sub>2</sub> MAX phase, the relative formation energy was calculated to be 0.039 eV/atom, while for the Ti<sub>3</sub>SnC<sub>2</sub>, it was 0.055 eV/atom. Furthermore, both Ti<sub>3</sub>AlC<sub>2</sub> and Ti<sub>3</sub>SnC<sub>2</sub> were predicted to have an exfoliation energy of 0.164 eV/Å<sup>2</sup>, suggesting that these MAX phases are comparable in terms of their possible etching. However, in our experiments, we did not observe an appreciable etching of tin from Ti<sub>3</sub>SnC<sub>2</sub> MAX phase using standard 48% HF (2 h) and MILD procedures for Ti<sub>3</sub>AlC<sub>2</sub>, as well as the modified procedure that is discussed further in this paper. Based on our results, even Ti<sub>3</sub>Al<sub>0.75</sub>Sn<sub>0.25</sub>C<sub>2</sub> is highly resistant to conventional etchants, despite containing only 25 atom % of Sn in the A-layers. It should be noted that we have also tried to etch Ti<sub>3</sub>Al<sub>0.75</sub>Sn<sub>0.25</sub>C<sub>2</sub> MAX phase crystals using concentrated HF for longer periods of time (up to 48 h); however, the results were not satisfactory and the etching products were heavily damaged; see Figure S1 in the Supporting Information.

Because of the decreased chemical reactivity of Ti<sub>3</sub>Al<sub>0.75</sub>Sn<sub>0.25</sub>C<sub>2</sub>, we had to develop a different chemical procedure that is considerably harsher compared to the conventional methods that are used for etching of Ti<sub>3</sub>AlC<sub>2</sub>. After testing numerous synthetic conditions, we ended up with a procedure that is schematically illustrated in Figure 3a. This is a two-step process that essentially combines both the 48% HF and the MILD methods in one procedure. We rationalize the effectiveness of this procedure for the complete removal of Al from Ti<sub>3</sub>Al<sub>0.75</sub>Sn<sub>0.25</sub>C<sub>2</sub> and producing a high-quality MXene material as follows. A prior comparison of the HF and the LiF-HCl procedures demonstrated that a concentrated HF might be too harsh as an etchant of Ti<sub>3</sub>AlC<sub>2</sub>, often overetching it and producing MXene flakes with pinholes. 45 Therefore, a LiF-HCl mixture could be advantageous as a milder etchant because it slowly produces HF in the reaction mixture in situ, as opposed to having a high concentration of HF from the beginning of the reaction. Another widely discussed benefit of a LiF-HCl mixture is that it produces bulky solvated Li<sup>+</sup> species that intercalate between the MXene layers once the reaction starts, exposing the interlayer spaces of the MAX phase particles for more efficient etching.

In the case of Ti<sub>3</sub>Al<sub>0.75</sub>Sn<sub>0.25</sub>C<sub>2</sub>, we employed the advantages of both methods. We first used a LiF-HCl mixture for 2 days to start the etching of the A-layers and initiate the intercalation of solvated Li<sup>+</sup> ions between the MXene layers. This intercalation facilitates further etching with a harsher etchant, 48% HF, which is needed for inert Ti<sub>3</sub>Al<sub>0.75</sub>Sn<sub>0.25</sub>C<sub>2</sub>. Due to the low reactivity of Ti<sub>3</sub>Al<sub>0.75</sub>Sn<sub>0.25</sub>C<sub>2</sub>, the 48% HF etching was performed for 4 days (in addition to the preliminary 2 day LiF-HCl etching) as opposed to 2 h needed to etch Al from Ti<sub>3</sub>AlC<sub>2</sub> (Figure 2c). Figure 3b demonstrates that shorter etching times were not sufficient. After 2 days of LiF-HCl etching and 1 day of 48% HF etching (the conditions that we refer to as 2D1D), the splitting of the layers in  $Ti_3Al_{0.75}Sn_{0.25}C_2$ particles becomes obvious, especially compared to the initial etching attempts (Figure 2d). Two additional days of 48% HF etching (the 2D3D conditions) extend the degree of etching of the MAX phase particles. Finally, 2 days of LiF-HCl etching and 4 days of 48% HF etching (the 2D4D conditions) result in a complete removal of Al from Ti<sub>3</sub>Al<sub>0.75</sub>Sn<sub>0.25</sub>C<sub>2</sub> and the formation of well-split Sn-Ti<sub>3</sub>C<sub>2</sub>T<sub>z</sub> MXene accordions (Figure 3b). Transmission electron microscopy (TEM) studies demonstrate that the Sn-Ti<sub>3</sub>C<sub>2</sub>T<sub>z</sub> MXene accordions prepared by the 2D4D method look similar to the Ti<sub>3</sub>C<sub>2</sub>T<sub>z</sub> MXene accordions produced from Ti<sub>3</sub>AlC<sub>2</sub> (Figure S2). Other etching conditions that we tested either did not produce MXene flakes from Ti<sub>3</sub>Al<sub>0.75</sub>Sn<sub>0.25</sub>C<sub>2</sub> or produced very defective materials (Figure S1). Moreover, the mechanical stirring can notably alter the synthesis yield (as shown in Figure S3), and uniform mixing is an important factor for producing high-quality MXene samples from  $Ti_3Al_{0.75}Sn_{0.25}C_2$ .

The removal of Al from Ti<sub>3</sub>Al<sub>0.75</sub>Sn<sub>0.25</sub>C<sub>2</sub> was monitored by EDX spectroscopy, and the results tracking the change in Al and Sn concentrations at different etching conditions are shown in Figure 3c. The initial two-day etching of Ti<sub>3</sub>Al<sub>0.75</sub>Sn<sub>0.25</sub>C<sub>2</sub> using the MILD method only slightly decreases the concentration of Al and leaves Sn practically unaffected. The concentration of Al in the MAX phase continues to gradually decrease as the sample is treated with 48% HF for one (2D1D) and 3 (2D3D) days until no aluminum is observed after 4 days in 48% HF (2D4D). Interestingly, Sn is also affected by the etching, although at a

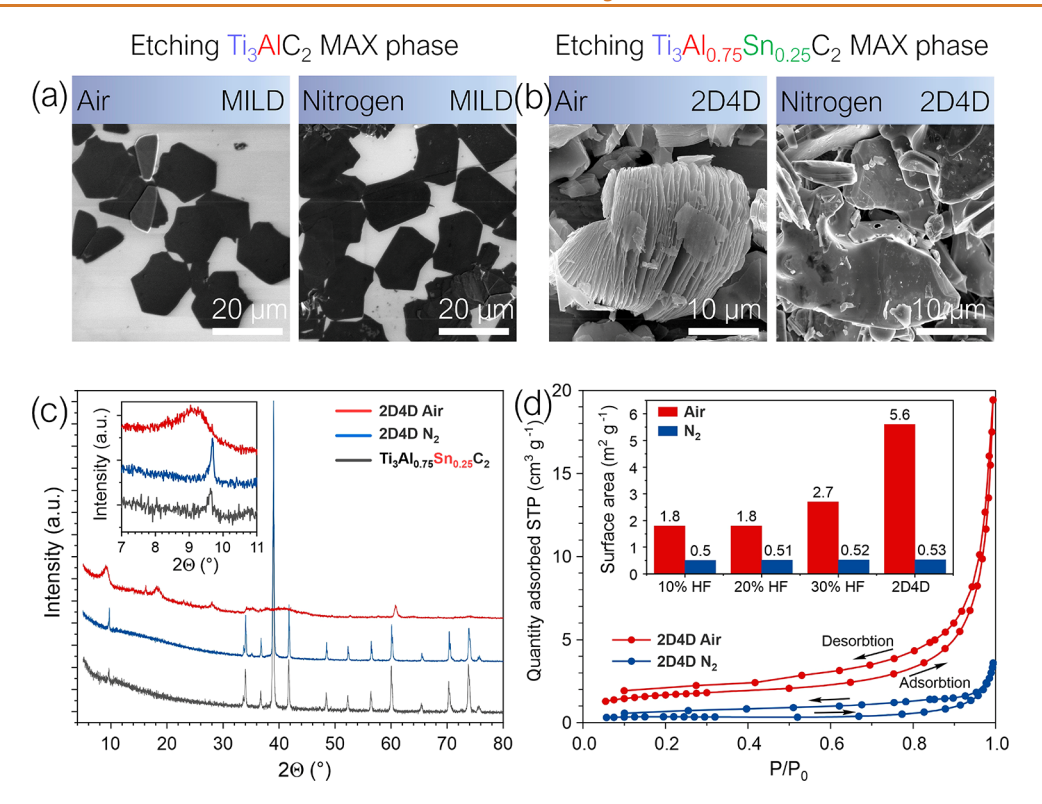


Figure 4. SEM, XRD, and BET analyses of etched  $Ti_3AlC_2$  and  $Ti_3Al_{0.75}Sn_{0.25}C_2$  MAX phases in air and  $N_2$ . (a) SEM images of  $Ti_3C_2T_z$  MXenes synthesized from the  $Ti_3AlC_2$  MAX phase by the MILD method in air (left) and nitrogen (right). (b) SEM images of the etching products of the  $Ti_3Al_{0.75}Sn_{0.25}C_2$  MAX phase prepared using the 2D4D method in air (left) and nitrogen (right). (c) XRD diffraction patterns of the  $Ti_3Al_{0.75}Sn_{0.25}C_2$  MAX phase (black) and its etching products prepared using the 2D4D method in air (red) and  $N_2$  (blue). (d) BET isotherms of the etching products of the  $Ti_3Al_{0.75}Sn_{0.25}C_2$  MAX phase prepared by the 2D4D method in air (red) and  $N_2$  (blue). The inset shows the surface areas of the etching products of the  $Ti_3Al_{0.75}Sn_{0.25}C_2$  MAX phase prepared by different methods in air and nitrogen.

much slower rate compared to aluminum, so that around 5 wt % (relative to the overall metal content) of tin remains in Sn- $Ti_3C_2T_z$  MXene at the end of the process. We also analyzed the Sn content using flame atomic absorption spectrometry (FAAS). The detection sensitivity of FAAS is well below the concentration of Sn in the MXene samples; therefore, it is a reliable method with a sensitivity of 1.7 mg L<sup>-1</sup> and a dynamic linear range (LDR) of 300 mg L<sup>-1</sup>. We dissolved 10 mg of Sn-Ti<sub>3</sub>C<sub>2</sub>T<sub>z</sub> MXene in aqua regia, and the final volume of the sample was 10 mL (after dilution). We measured three different batches of samples. According to our analysis, the Sn content was 46  $\pm$  1.8  $\mu$ g mL<sup>-1</sup> (44–48 ppm), which is equivalent to 4.42-4.78% of the initial weight (close to 5%). Thus, the EDX and FAAS analyses produced comparable results on the tin content in Sn-Ti<sub>3</sub>C<sub>2</sub>T<sub>z</sub> MXene. It should be noted that the Sn content of about ~5 wt % in Sn-Ti<sub>3</sub>C<sub>2</sub>T<sub>z</sub> MXene determined by EDX is based on the metal content and excludes the mass of carbons and Tz groups, and if light elements could be accurately accounted for by the EDX analysis, the EDX and FAAS results would likely be even closer to each other.

Importantly, tin is very uniformly distributed over the Sn— ${\rm Ti}_3{\rm C}_2{\rm T}_z$  particles, as shown by SEM and EDX mapping data in Figure 3d,e, which is caused by the uniform distribution of Sn within the A-layers of  ${\rm Ti}_3{\rm Al}_{0.75}{\rm Sn}_{0.25}{\rm C}_2$ . The uniform modification of MXene layers with an A-element is one of the advantages of the proposed method (Figure 1b) compared to other possible approaches for MXene modification based on, for example, electrochemical deposition or sol—gel

chemistry, which often result in nonuniform nucleation of nanoparticles at the edges and defect sites of the flakes.

Our experiments on the optimization of etching conditions for Ti<sub>3</sub>Al<sub>0.75</sub>Sn<sub>0.25</sub>C<sub>2</sub> MAX phase revealed a peculiar role that oxygen plays in the process. We found that oxygen from air is not necessary for etching of Ti<sub>3</sub>AlC<sub>2</sub>, but it is a critical factor for etching of the Sn-modified MAX phase. To demonstrate the effect, we etched Ti<sub>3</sub>AlC<sub>2</sub> and Ti<sub>3</sub>Al<sub>0.75</sub>Sn<sub>0.25</sub>C<sub>2</sub> MAX phases using the optimized conditions in air and then repeated the processes with nitrogen being bubbled through the etching solutions to displace oxygen. The results of these experiments are summarized in Figure 4. SEM images in Figure 4a compare the Ti<sub>3</sub>C<sub>2</sub>T<sub>z</sub> MXene flakes synthesized using the MILD method with (air, left panel) and without (N2, right panel) the presence of oxygen. The visual comparison of these images suggests that the etching process is not affected by the change in the reaction atmosphere. SEM images in Figure 4b compare the products of etching of the Ti<sub>3</sub>Al<sub>0.75</sub>Sn<sub>0.25</sub>C<sub>2</sub> MAX phase using the 2D4D method with and without oxygen, and the difference is significant. Crystals of the Ti<sub>3</sub>Al<sub>0.75</sub>Sn<sub>0.25</sub>C<sub>2</sub> MAX phase that have been etched in air produced particles with a well-etched accordion-like morphology (left panel in Figure 4b). However, in contrast to the air environment, crystals etched in N<sub>2</sub> do not exhibit any visible morphological change (right panel in Figure 4b). According to the results of the EDX analysis presented in Table S1, the crystals etched in N2 do not exhibit any significant change in their Al content, which remains comparable to that in the parent MAX phase (about 13.5 wt %). The Sn-Ti<sub>3</sub>C<sub>2</sub>T<sub>z</sub> samples produced in ambient conditions, on the other hand, showed the complete etching of

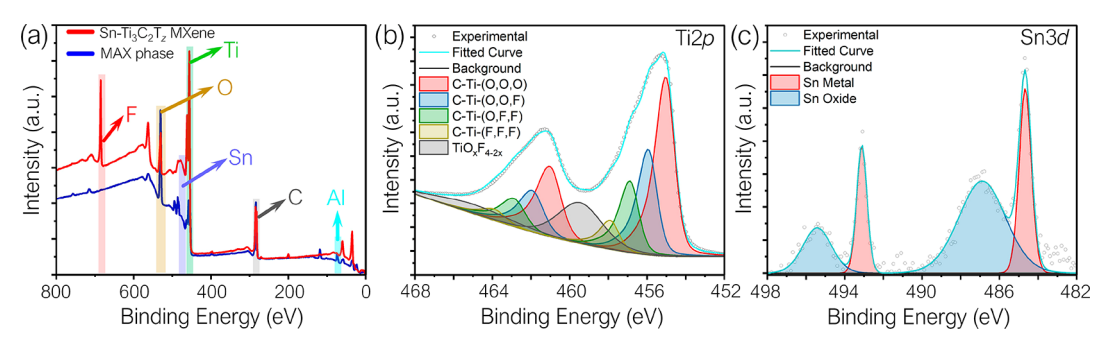


Figure 5. XPS analysis of  $Sn-Ti_3C_2T_z$  MXene. (a) XPS survey spectra for the  $Ti_3Al_{0.75}Sn_{0.25}C_2$  MAX phase (blue) and  $Sn-Ti_3C_2T_z$  MXene (red). (b) High-resolution XPS Ti2p spectrum of  $Sn-Ti_3C_2T_z$  MXene. (c) High-resolution XPS Sn3d spectrum of  $Sn-Ti_3C_2T_z$  MXene.

Al. The same trend regarding the effect of the reaction atmosphere was observed for other etchants tested in this study (10%, 20%, and 30% HF), and the SEM images of the etching products from these experiments are summarized in Figures S4–S6.

The results of XRD and Brunauer-Emmett-Teller (BET) surface area analysis also demonstrate the difference in the etching behavior of Ti<sub>3</sub>AlC<sub>2</sub> and Ti<sub>3</sub>Al<sub>0.75</sub>Sn<sub>0.25</sub>C<sub>2</sub> MAX phases (Figures 4c,d, S7, and S8). As evident from the comparison of the XRD patterns in Figure 4c, the Ti<sub>3</sub>Al<sub>0.75</sub>Sn<sub>0.25</sub>C<sub>2</sub> MAX phase etched in ambient conditions using the 2D4D protocol (red line in Figure 4c) shows a successful etching process with the prominent peaks of Sn-Ti<sub>3</sub>C<sub>2</sub>T<sub>z</sub> at 9.1°, 18.3°, and 27.5° indexed as (001), (002), and (003), respectively. However, the XRD pattern of the sample etched under N<sub>2</sub> (blue line) is almost indistinguishable from the XRD pattern of the parent MAX phase (black line). Figure 4d presents the results of textural properties analysis, showing one order of magnitude increase in N2 gas adsorption and surface area (Figure 4d, inset) for the product of the etching of  $Ti_3Al_{0.75}Sn_{0.25}C_2$  (the 2D4D method, ambient conditions) compared to the parent MAX phase. Similar to the XRD data, the samples etched under N<sub>2</sub> were comparable to the parent MAX phase in terms of their gas adsorption and surface area characteristics.

The synthesis of  $Sn-Ti_3C_2T_z$  from  $Ti_3Al_{0.75}Sn_{0.25}C_2$  is accompanied by the etching of all Al and a considerable amount of Sn, whose content, if presented in terms of the Sn/ Ti weight ratio, decreases from 0.17 in the precursor MAX phase to about 0.06 in the final MXene using the 2D4D conditions; see Table S1. Therefore, the difference between the etching behavior of Ti<sub>3</sub>AlC<sub>2</sub> and Ti<sub>3</sub>Al<sub>0.75</sub>Sn<sub>0.25</sub>C<sub>2</sub> MAX phases suggests that unlike aluminum, tin cannot be easily etched from the A-layers of a MAX phase using HF only and a secondary reagent, such as oxygen, is necessary. In general, the HF etching of layered Ti<sub>3</sub>AlC<sub>2</sub> particles starts at the exposed edges of the layers, and a layer opening is necessary for the etching to proceed, so that HF could intercalate between the split Ti<sub>3</sub>C<sub>2</sub> layers and react with Al in the bulk of the particles.<sup>49</sup> As we demonstrate in this study, for Ti<sub>3</sub>AlC<sub>2</sub>, the HF etching does not require oxygen. However, if Ti<sub>3</sub>Al<sub>0.75</sub>Sn<sub>0.25</sub>C<sub>2</sub> is treated with HF without oxygen, there is a large number of Sn atoms in the A-layers that cannot be etched, and as a result, the unreacted tin between the Ti<sub>3</sub>C<sub>2</sub> layers keeps them close and prevents the layer opening. Correspondingly, HF cannot access the aluminum inside the Ti<sub>3</sub>Al<sub>0.75</sub>Sn<sub>0.25</sub>C<sub>2</sub> particles, and the MAX phase remains unetched, as we observed experimentally. In contrast, in the presence of oxygen, both Al and Sn are being etched from

 $Ti_3Al_{0.75}Sn_{0.25}C_2$  in a HF solution, though at very different rates; see Figure 3c.

In general, tin is a less reactive metal than aluminum, and it is, therefore, reasonable that Ti<sub>3</sub>Al<sub>0.75</sub>Sn<sub>0.25</sub>C<sub>2</sub> is more difficult to etch compared to Ti<sub>3</sub>AlC<sub>2</sub>. This general difference in the reactivities of the two elements can be further amplified by the fact that their etching should occur in the confined space between the Ti<sub>3</sub>C<sub>2</sub> layers. As we point out in the discussion of the XRD data, a Sn atom perfectly fits in a trigonal prism formed by six titanium atoms, while a smaller Al is loose in this cavity, which makes it more accessible to the reagents. Noteworthy, there is an apparent analogy between the observed effect of oxygen on the etchability of Ti<sub>3</sub>Al<sub>0.75</sub>Sn<sub>0.25</sub>C<sub>2</sub> MAX phase in HF and the earlier report on Ti<sub>3</sub>C<sub>2</sub>T<sub>7</sub> MXene synthesis from Ti<sub>3</sub>SiC<sub>2</sub>.<sup>50</sup> It was demonstrated that the concentrated HF alone cannot be used for etching Si from Ti<sub>3</sub>SiC<sub>2</sub> MAX phase, but various HF/oxidant mixtures, where an oxidant could be H<sub>2</sub>O<sub>2</sub>, (NH<sub>4</sub>)<sub>2</sub>S<sub>2</sub>O<sub>8</sub>, KMnO<sub>4</sub>, FeCl<sub>3</sub>, and HNO<sub>3</sub>, were shown to be effective.  $^{50}$  Sn is in the same group of the Periodic Table as Si, and it is noteworthy that the Ti<sub>3</sub>Al<sub>0.75</sub>Sn<sub>0.25</sub>C<sub>2</sub> MAX phase also requires an oxidant, such as O2, in addition to HF for a successful etching. The role of an oxidant is related to the fact that in the process of HF etching, an A-element forms a soluble fluoride, in which it is in an oxidized rather than its original metallic form. The discussed experimental data suggest that Al is sufficiently reactive to be etched by HF even in a confined space between the Ti<sub>3</sub>C<sub>2</sub> layers, while both Si and Sn have higher electronegativities and require an additional oxidant to facilitate their transition to soluble fluorides.

As we discussed in the Introduction, the synthesis of A"- $M_{n+1}X_nT_z$  MXenes from  $M_{n+1}A'_{1-x}A''_xX_n$  MAX phases can result in many interesting combinations of MXenes with various A-elements that could find applications in various fields, such as catalysis, energy storage, and gas sensing. However, in addition to these potentially anticipated outcomes, we also found two unexpected behaviors of Sn-Ti<sub>3</sub>C<sub>2</sub>T<sub>z</sub> that also offer practical benefits. First of all, our data suggest that Sn-Ti<sub>3</sub>C<sub>2</sub>T<sub>z</sub> has significantly improved environmental stability compared to the unmodified MXene. Ti<sub>3</sub>C<sub>2</sub>T<sub>2</sub> is known to degrade even under the established conditions of few-hour etching that often result in flakes with pinholes and oxide nanoparticles. 31,45 Here, Sn-Ti<sub>3</sub>C<sub>2</sub>T<sub>z</sub> produced by the 2D4D method was exposed to extremely harsh acidic conditions for a total of 6 days, and the resulting flakes looked clean and uniform. A possible explanation for the improved environmental stability of Sn-Ti<sub>3</sub>C<sub>2</sub>T<sub>z</sub> could be related to the passivating role of the chemically inert Sn species that may

terminate the defect sites in the MXene layers where oxidation would have started without such passivation. <sup>29,32</sup>

XPS analysis was performed to investigate the quality of the produced Sn-Ti<sub>3</sub>C<sub>2</sub>T<sub>z</sub> MXene, and the results are summarized in Figure 5. The XPS survey spectrum of the parent Ti<sub>3</sub>Al<sub>0.75</sub>Sn<sub>0.25</sub>C<sub>2</sub> MAX phase is shown in Figure 5a and confirms the presence of Ti, Sn, Al, and C. In comparison, due to the surface functionalization during the HF etching, the XPS survey spectrum of Sn-MXene reveals an additional peak for the terminal fluorine groups, while the Al peak disappears. Despite the prolonged etching in concentrated HF for a total of 6 days (144 h), the XPS Ti2p spectrum of Sn-MXene in Figure 5b does not show a pronounced TiO<sub>2</sub> peak, suggesting the stability of the material under very harsh acidic conditions. The spectrum was analyzed using the Fit-V protocol described by Barsoum and co-workers,  $^{51}$  with different  $Ti2p_{3/2}$ components assigned to Ti atoms in various octahedral environments in MXene structure, such as C-Ti-(O,O,O) (455.1 eV), C-Ti-(O,O,F) (456.0 eV), C-Ti-(O,F,F)(457.0 eV), and C-Ti-(F,F,F) (457.9 eV), while the peak at 459.6 eV was assigned to  $TiO_{2-x}F_{2x}$ . The separation  $\Delta_{Ti2p}$ between the Ti2 $p_{1/2}$  and Ti 2 $p_{3/2}$  peaks was kept consistent for all components and set to  $6.1 \pm 0.15$  eV, and the fitting peaks are asymmetric because of the high conductivity of Ti<sub>3</sub>C<sub>2</sub>T<sub>2</sub> MXene. 51 For a comparison, we also show XPS Ti2p spectrum of Ti<sub>3</sub>C<sub>2</sub>T<sub>z</sub> MXene that was subjected to the same prolonged 48% HF etching (144 h) using the 2D4D procedure; see Figure S9. While the oxide peak at 459.6 eV ( $TiO_{2-x}F_{2x}$ ) is only revealed as a fitting component for Sn-Ti<sub>3</sub>C<sub>2</sub>T<sub>z</sub>, it is very prominent for Ti<sub>3</sub>C<sub>2</sub>T<sub>z</sub> treated under the same conditions, demonstrating the improved chemical stability of the Snmodified MXene. Another manifestation of a higher degree of oxidation of  $Ti_3C_2T_z$  is the broad satellite oxide peak between 470 and 475 eV (Figure S9b) that is not observed for Sn-Ti<sub>3</sub>C<sub>2</sub>T<sub>2</sub>. The XPS spectra in Figure S9 are also supplemented with representative SEM images, which show the degradation of Ti<sub>3</sub>C<sub>2</sub>T<sub>z</sub> compared to Sn-Ti<sub>3</sub>C<sub>2</sub>T<sub>z</sub>.

The high-resolution XPS Sn3d spectrum of Sn-Ti<sub>3</sub>C<sub>2</sub>T<sub>z</sub> MXene in Figure 5c demonstrates the presence of both elemental Sn and its oxide forms (SnO<sub>x</sub>). As there was no microscopic evidence for an aggregation of Sn and SnO<sub>x</sub> (Figure 3d,e), these species should be present in a nanoscopic form, which would be of significant benefit for various applications, such as gas sensing and energy storage. <sup>29,32,33,36</sup>

Another interesting observation regarding the behavior of  $Sn-Ti_3C_2T_z$  is the dramatic electrostatic expansion of the MXene accordions that we frequently observed during their SEM imaging. This behavior is schematically illustrated in Figure 6a, which explains the progression of SEM images recorded on the same Sn-Ti<sub>3</sub>C<sub>2</sub>T<sub>z</sub> accordion over a period of 10 s; see Figure 6b. As the electron beam of a microscope irradiates the accordion particle, it charges the MXene layers that spatially separate because of the electrostatic repulsion. This electrostatic behavior could be facilitated by the presence of wide-bandgap semiconductor SnO<sub>x</sub> species in the interlayer spaces within the accordions, which hampers the charge sinking from MXene layers. Practically, the electrostatically driven elongation of Sn-Ti<sub>3</sub>C<sub>2</sub>T<sub>z</sub> accordions by over 100% of their length could provide an interesting platform for MXenebased NEMS devices. 41-43 Figure 6c,d demonstrates SEM images of other Sn-MXene particles showing the same electrostatic behavior and exfoliation of the accordions into thin flakes.

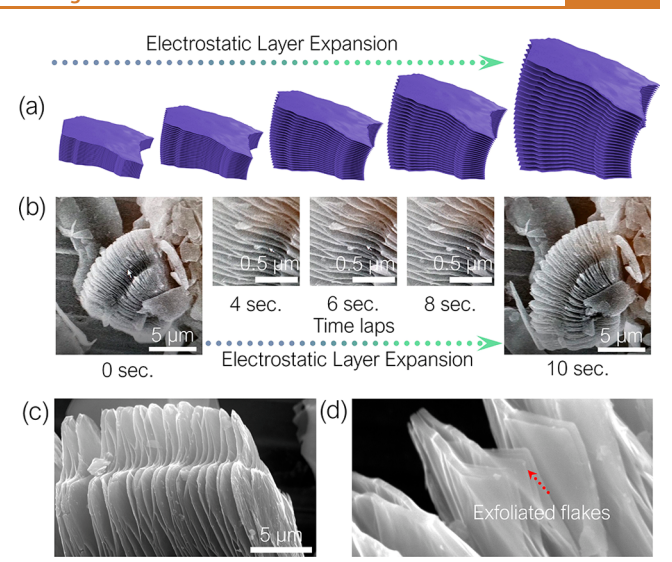


Figure 6. Electrostatic expansion of accordion-like  $Sn-Ti_3C_2T_z$  MXene particles deposited on a Cu foil substrate. (a) Animation and (b) SEM images of the electrostatic expansion of a  $Sn-Ti_3C_2T_z$  MXene accordion under an electron beam; the particle expands into a highly extended structure. The small arrows show the same position in the accordion. (c, d) SEM images of Sn-MXene crystals showing separated MXene flakes after the electrostatic expansion.

Noteworthy, the Sn-Ti $_3$ C $_2$ T $_z$  MXene does not necessarily have to be used in a form of the accordion-like particles. These accordions can be exfoliated using tetramethylammonium hydroxide (TMAOH) as an intercalant and a sonication for 30 min, forming stable colloidal solutions in water (Figure S10). These solutions contain monolayer and few-layer flakes that can be processed into uniform thin films (Figure S10). Such films are a standard test bed in the field of MXenes for studying them for a variety of applications in energy storage, scatalysis, as sensors, selectromagnetic interference shielding, set. Many of these applications may benefit from modification of MXenes with some of the A-elements, either in metallic or oxide form, and could therefore employ various A-MXenes prepared using the general strategy disclosed in this work.

### **CONCLUSIONS**

In summary, we discussed a synthetic strategy for A-MXenes, in which an A-element modifies the interlayer spaces of MXene flakes in the form of metallic species or oxides, depending on its chemical identity and conditions. The proposed strategy for A-MXenes relies on the synthesis of a MAX phase with more than one A-element, such as  $M_{n+1}A'_{1-x}A''_xX_n$  MAX phase, in which the higher reactivity of the A'-element compared to A" enables its selective etching, resulting in A"- $M_{n+1}X_nT_z$ . We discuss the advantages of this strategy and demonstrate its viability by synthesizing Sn-modified Ti<sub>3</sub>C<sub>2</sub>T<sub>z</sub> MXene from the Ti<sub>3</sub>Al<sub>0.75</sub>Sn<sub>0.25</sub>C<sub>2</sub> MAX phase. Although the incorporation of Sn in the A-layer of Ti<sub>3</sub>AlC<sub>2</sub> decreases the MAX phase reactivity, we developed an etching procedure to completely remove Al and produce Sn-Ti<sub>3</sub>C<sub>2</sub>T<sub>z</sub> MXene. The resulting MXene sheets were of very high quality and exhibited improved environmental stability, which we attribute to the effect of uniform Sn modification. Finally, we demonstrate a peculiar electrostatic expansion of Sn-Ti<sub>3</sub>C<sub>2</sub>T<sub>z</sub> accordions, which may find interesting applications in MXene-based nano-electromechanical systems. Overall, these results demonstrate that in addition to different combinations of M and X elements in MAX phases there is a great potential for the synthesis of MXene materials based on the utilization of multiple elements in the A-layer. The generality of this proposed method should be further explored by testing various combinations of A-elements other than Al and Sn.

### **EXPERIMENTAL SECTION**

**Materials.** Ti (99%, 325 mesh), Al (99%, 325 mesh), and TiC (99.9%, 325 mesh) were purchased from Alfa Aesar. Sn (99.5%, 100 mesh) was purchased from Sigma-Aldrich. HCl and HF were purchased from VWR, and LiF was purchased from Spectrum Chemical and used as received. Potassium carbonate was purchased from Sigma-Aldrich and used to neutralize acids.

**Synthesis.** Ti<sub>3</sub>AlC<sub>2</sub> MAX phase was synthesized according to the previously reported procedure. <sup>57</sup> In brief, TiC, Ti, and Al were mixed at a molar ratio of 2:1:1.2 using a pestle and mortar and annealed at 1450 °C for 4 h under the flow of Ar (300 sccm). The same approach was taken for the synthesis of Ti<sub>3</sub>Al<sub>0.75</sub>Sn<sub>0.25</sub>C<sub>2</sub> MAX phase, with the molar ratio being 2:1:0.85:0.25 for TiC/Ti/Al/Sn. An excess of aluminum to the stoichiometry is required to compensate for its evaporation during annealing at high temperatures.

MXene samples were synthesized from the corresponding MAX phases by several methods that included the HF etching,<sup>5</sup> the MILD method,<sup>45</sup> and the optimized two-step synthesis method (Figure 3). For the HF method, 500 mg of the MAX phase powder was slowly added to 10 mL of an aqueous solution of HF (10, 20, 30, or 48%), and the mixture was stirred for different periods of time that ranged from 2 to 48 h. Then, the samples were centrifuged and washed with deionized (DI) water until pH 6 was reached.

For the MILD synthesis method, 500 mg of the MAX phase was slowly dispersed in the mixture of LiF (800 mg) and 9 M HCl (10 mL) and stirred for 24 h. After the synthesis, the samples were washed with DI water until pH 6 was reached and delaminated into flakes by shaking for 15 min.

For the optimized two-step synthesis method, denoted as 2D4D, the MAX phase crystals were first etched for 48 h in the mixture of LiF in HCl (500 mg of MAX phase, 800 mg of LiF, 35 mL of 9 M HCl). After 48 h, samples were centrifuged and without further processing subjected to an additional 96 h etching in 48% HF (10 mL). When the synthesis was finished, the samples were centrifuged and washed with DI water until pH 6 was reached.

Characterization. The morphology of the samples was studied by SEM using an FEI Nova NanoSEM 450 instrument with an EDX analysis capability. Ti<sub>3</sub>C<sub>2</sub>T<sub>z</sub> powder was sonicated in dehydrated ethanol for 1 min and drop cast on a substrate, dried in air, and loaded into the SEM instrument. TEM images were collected by using an FEI Tecnai Osiris instrument (200 kV) on MXene particles deposited on lacey carbon TEM grids. The textural properties of the samples were determined from the nitrogen adsorption isotherms recorded at -196 °C using a Micrometrics ASAP 2460 Accelerated Surface Area and Porosimetry Analyzer. Before performing the adsorption experiments, all samples were dried at 180 °C for 48 h under N2. The standard BET procedure was used to calculate the specific surface areas of the samples. The amount of nitrogen adsorbed at a relative pressure of 0.985 was used to estimate the total pore volume. The Sn content in Sn-Ti<sub>3</sub>C<sub>2</sub>T<sub>z</sub> MXene was analyzed by a 3100 PerkinElmer FAAS instrument in an air-acetylene flame, according to the user manual. XRD patterns were recorded with a PANalytical Empyrean powder diffractometer with Ni-filtered Cu K $\alpha$  radiation operated at 40 kV and 30 mA. A step size of  $0.03^{\circ}$  and 1 s dwelling times were used to collect the XRD patterns. Quantitative Rietveld refinements of the powder XRD patterns were performed using JANA2006 software, 58 employing internal tables for X-ray atomic form factors. XPS of the samples was performed at room temperature on a Thermo Scientific K-Alpha X-ray photoelectron spectrometer using a monochromated Al K $\alpha$ (1486.6 eV) X-ray source and a low energy electron flood gun for

charge neutralization. The high-resolution Ti2p and Sn3d spectra were collected using a pass energy of 20 eV and a 0.1 eV step.

### ASSOCIATED CONTENT

# **Supporting Information**

The Supporting Information is available free of charge at https://pubs.acs.org/doi/10.1021/acsnano.3c02198.

Additional electron microscopy images of the etching products of  $Ti_3AlC_2$  and  $Ti_3Al_{0.75}Sn_{0.25}C_2$  MAX phases (Figures S1–S6); XRD data for  $Ti_3Al_{0.75}Sn_{0.25}C_2$  MAX phase and its etching products prepared under different conditions (Figure S7); BET data for  $Ti_3Al_{0.75}Sn_{0.25}C_2$  MAX phase and its etching products prepared under different conditions (Figure S8); a comparison of XPS and SEM data for MXenes produced by etching  $Ti_3Al_{0.75}Sn_{0.25}C_2$  and  $Ti_3AlC_2$  MAX phases using the 2D4D method (Figure S9); optical photographs and SEM images illustrating the delamination of Sn— $Ti_3C_2T_z$  MXene and its processing into thin films (Figure S10); EDX data for the etching products of  $Ti_3Al_{0.75}Sn_{0.25}C_2$  MAX phase in air and  $N_2$  (Table S1) (PDF)

# **AUTHOR INFORMATION**

### **Corresponding Author**

Alexander Sinitskii — Department of Chemistry and Nebraska Center for Materials and Nanoscience, University of Nebraska-Lincoln, Lincoln, Nebraska 68588, United States; orcid.org/0000-0002-8688-3451; Email: sinitskii@ unl.edu

# Authors

Saman Bagheri — Department of Chemistry, University of Nebraska-Lincoln, Lincoln, Nebraska 68588, United States; orcid.org/0000-0002-4206-3021

Alexey Lipatov — Department of Chemistry, University of Nebraska-Lincoln, Lincoln, Nebraska 68588, United States; Department of Chemistry, Biology, and Health Sciences and Karen M. Swindler Department of Chemical and Biological Engineering, South Dakota School of Mines and Technology, Rapid City, South Dakota 57701, United States;

orcid.org/0000-0001-5043-1616

Nataliia S. Vorobeva – Department of Chemistry, University of Nebraska-Lincoln, Lincoln, Nebraska 68588, United States

Complete contact information is available at: https://pubs.acs.org/10.1021/acsnano.3c02198

# **Author Contributions**

S.B. and A.S. designed the project. S.B. carried out most of the experiments including materials synthesis and characterization. A.L. analyzed the XRD results. N.V.S. performed the XPS analysis. S.B. and A.L. prepared the figures. S.B., A.L., and A.S. wrote the manuscript. A.S. supervised the project.

### Notes

The authors declare no competing financial interest.

# **ACKNOWLEDGMENTS**

The work was supported by the Nebraska Center for Energy Sciences Research (NCESR) and the National Science Foundation (NSF) through EPSCoR RII Track-1: Emergent Quantum Materials and Technologies (EQUATE), award OIA-2044049. Some experiments were performed using the

instrumentation at the Nebraska Nanoscale Facility, which is supported by the National Science Foundation (NSF ECCS-2025298) and the Nebraska Research Initiative.

### **REFERENCES**

- (1) Gogotsi, Y.; Anasori, B. The Rise of MXenes. ACS Nano 2019, 13 (8), 8491-8494.
- (2) Anasori, B.; Gogotsi, Y. 2D Metal Carbides and Nitrides (MXenes): Structure, Properties and Applications; Springer International Publishing, 2019.
- (3) Eklund, P.; Beckers, M.; Jansson, U.; Högberg, H.; Hultman, L. The  $M_{n+1}AX_n$  phases: Materials science and thin-film processing. *Thin Solid Films* **2010**, *518* (8), 1851–1878.
- (4) Barsoum, M. W. The  $M_{N+1}A_XN$  phases: A new class of solids: Thermodynamically stable nanolaminates. *Prog. Solid State Chem.* **2000**, 28 (1), 201–281.
- (5) Naguib, M.; Kurtoglu, M.; Presser, V.; Lu, J.; Niu, J.; Heon, M.; Hultman, L.; Gogotsi, Y.; Barsoum, M. W. Two-Dimensional Nanocrystals Produced by Exfoliation of Ti<sub>3</sub>AlC<sub>2</sub>. *Adv. Mater.* **2011**, 23 (37), 4248–4253.
- (6) Alhabeb, M.; Maleski, K.; Anasori, B.; Lelyukh, P.; Clark, L.; Sin, S.; Gogotsi, Y. Guidelines for Synthesis and Processing of Two-Dimensional Titanium Carbide (Ti<sub>3</sub>C<sub>2</sub>T<sub>x</sub> MXene). *Chem. Mater.* **2017**, 29 (18), 7633–7644.
- (7) Lipatov, A.; Goad, A.; Loes, M. J.; Vorobeva, N. S.; Abourahma, J.; Gogotsi, Y.; Sinitskii, A. High electrical conductivity and breakdown current density of individual monolayer Ti<sub>3</sub>C<sub>2</sub>T<sub>x</sub> MXene flakes. *Matter* **2021**, *4* (4), 1413–1427.
- (8) Seh, Z. W.; Fredrickson, K. D.; Anasori, B.; Kibsgaard, J.; Strickler, A. L.; Lukatskaya, M. R.; Gogotsi, Y.; Jaramillo, T. F.; Vojvodic, A. Two-Dimensional Molybdenum Carbide (MXene) as an Efficient Electrocatalyst for Hydrogen Evolution. *ACS Energy Letters* **2016**, *1* (3), 589–594.
- (9) Soundiraraju, B.; George, B. K. Two-Dimensional Titanium Nitride (Ti<sub>2</sub>N) MXene: Synthesis, Characterization, and Potential Application as Surface-Enhanced Raman Scattering Substrate. *ACS Nano* **2017**, *11* (9), 8892–8900.
- (10) Hantanasirisakul, K.; Alhabeb, M.; Lipatov, A.; Maleski, K.; Anasori, B.; Salles, P.; Ieosakulrat, C.; Pakawatpanurut, P.; Sinitskii, A.; May, S. J.; Gogotsi, Y. Effects of Synthesis and Processing on Optoelectronic Properties of Titanium Carbonitride MXene. *Chem. Mater.* **2019**, *31* (8), 2941–2951.
- (11) Mashtalir, O.; Lukatskaya, M. R.; Zhao, M.-Q.; Barsoum, M. W.; Gogotsi, Y. Amine-Assisted Delamination of Nb<sub>2</sub>C MXene for Li-Ion Energy Storage Devices. *Adv. Mater.* **2015**, 27 (23), 3501–3506.
- (12) Ghidiu, M.; Naguib, M.; Shi, C.; Mashtalir, O.; Pan, L. M.; Zhang, B.; Yang, J.; Gogotsi, Y.; Billinge, S. J. L.; Barsoum, M. W. Synthesis and characterization of two-dimensional Nb<sub>4</sub>C<sub>3</sub> (MXene). *Chem. Commun.* **2014**, *50* (67), 9517–9520.
- (13) Lipatov, A.; Alhabeb, M.; Lu, H.; Zhao, S.; Loes, M. J.; Vorobeva, N. S.; Dall'Agnese, Y.; Gao, Y.; Gruverman, A.; Gogotsi, Y.; Sinitskii, A. Electrical and Elastic Properties of Individual Single-Layer Nb<sub>4</sub>C<sub>3</sub>T<sub>x</sub> MXene Flakes. *Advanced Electronic Materials* **2020**, *6* (4), No. 1901382.
- (14) Wu, M.; Wang, B. X.; Hu, Q. K.; Wang, L. B.; Zhou, A. G. The Synthesis Process and Thermal Stability of  $V_2C$  MXene. *Materials* **2018**, 11 (11), 2112.
- (15) Shan, Q.; Mu, X.; Alhabeb, M.; Shuck, C. E.; Pang, D.; Zhao, X.; Chu, X.-F.; Wei, Y.; Du, F.; Chen, G.; Gogotsi, Y.; Gao, Y.; Dall'Agnese, Y. Two-dimensional vanadium carbide (V<sub>2</sub>C) MXene as electrode for supercapacitors with aqueous electrolytes. *Electrochem. Commun.* **2018**, *96*, 103–107.
- (16) Hantanasirisakul, K.; Anasori, B.; Nemsak, S.; Hart, J. L.; Wu, J.; Yang, Y.; Chopdekar, R. V.; Shafer, P.; May, A. F.; Moon, E. J.; Zhou, J.; Zhang, Q.; Taheri, M. L.; May, S. J.; Gogotsi, Y. Evidence of a magnetic transition in atomically thin  $Cr_2TiC_2T_x$  MXene. *Nanoscale Horizons* **2020**, *S* (12), 1557–1565.

- (17) Deysher, G.; Shuck, C. E.; Hantanasirisakul, K.; Frey, N. C.; Foucher, A. C.; Maleski, K.; Sarycheva, A.; Shenoy, V. B.; Stach, E. A.; Anasori, B.; Gogotsi, Y. Synthesis of Mo<sub>4</sub>VAlC<sub>4</sub> MAX Phase and Two-Dimensional Mo<sub>4</sub>VC<sub>4</sub> MXene with Five Atomic Layers of Transition Metals. *ACS Nano* **2020**, *14* (1), 204–217.
- (18) Nemani, S. K.; Zhang, B.; Wyatt, B. C.; Hood, Z. D.; Manna, S.; Khaledialidusti, R.; Hong, W.; Sternberg, M. G.; Sankaranarayanan, S. K. R. S.; Anasori, B. High-Entropy 2D Carbide MXenes: TiVNbMoC<sub>3</sub> and TiVCrMoC<sub>3</sub>. ACS Nano **2021**, 15 (8), 12815–12825.
- (19) Li, M.; Lu, J.; Luo, K.; Li, Y.; Chang, K.; Chen, K.; Zhou, J.; Rosen, J.; Hultman, L.; Eklund, P.; Persson, P. O. A.; Du, S.; Chai, Z.; Huang, Z.; Huang, Q. Element Replacement Approach by Reaction with Lewis Acidic Molten Salts to Synthesize Nanolaminated MAX Phases and MXenes. *J. Am. Chem. Soc.* **2019**, *141* (11), 4730–4737. (20) Li, Y.; Lu, J.; Li, M.; Chang, K.; Zha, X.; Zhang, Y.; Chen, K.; Persson, P. O. A.; Hultman, L.; Eklund, P.; Du, S.; Francisco, J. S.;
- Persson, P. O. A.; Hultman, L.; Eklund, P.; Du, S.; Francisco, J. S.; Chai, Z.; Huang, Z.; Huang, Q. Multielemental single-atom-thick A layers in nanolaminated  $V_2(Sn, A)$  C (A = Fe, Co, Ni, Mn) for tailoring magnetic properties. *Proc. Natl. Acad. Sci. U. S. A.* **2020**, 117 (2), 820–825.
- (21) Hermawan, A.; Zhang, B.; Taufik, A.; Asakura, Y.; Hasegawa, T.; Zhu, J. F.; Shi, P.; Yin, S. CuO Nanoparticles/Ti<sub>3</sub>C<sub>2</sub>T<sub>x</sub> MXene Hybrid Nanocomposites for Detection of Toluene Gas. *ACS Appl. Nano Mater.* **2020**, *3* (5), 4755–4766.
- (22) Saini, B.; Harikrishna, K.; Laishram, D.; Krishnapriya, R.; Singhal, R.; Sharma, R. K. Role of ZnO in ZnO Nanoflake/Ti<sub>3</sub>C<sub>2</sub> MXene Composites in Photocatalytic and Electrocatalytic Hydrogen Evolution. *ACS Appl. Nano Mater.* **2022**, *5* (7), 9319–9333.
- (23) Yu, X. L.; Wang, T.; Yin, W. C.; Zhang, Y. H. Ti<sub>3</sub>C<sub>2</sub> MXene nanoparticles modified metal oxide composites for enhanced photoelectrochemical water splitting. *Int. J. Hydrogen Energy* **2019**, 44 (5), 2704–2710.
- (24) Chaudhari, N. K.; Jin, H.; Kim, B.; San Baek, D.; Joo, S. H.; Lee, K. MXene: an emerging two-dimensional material for future energy conversion and storage applications. *J. Mater. Chem. A* **2017**, 5 (47), 24564–24579.
- (25) Zhu, J.; Ha, E.; Zhao, G.; Zhou, Y.; Huang, D.; Yue, G.; Hu, L.; Sun, N.; Wang, Y.; Lee, L. Y. S.; Xu, C.; Wong, K.-Y.; Astruc, D.; Zhao, P. Recent advance in MXenes: A promising 2D material for catalysis, sensor and chemical adsorption. *Coord. Chem. Rev.* **2017**, 352, 306–327.
- (26) Jun, B. M.; Kim, S.; Heo, J.; Park, C. M.; Her, N.; Jang, M.; Huang, Y.; Han, J.; Yoon, Y. Review of MXenes as new nanomaterials for energy storage/delivery and selected environmental applications. *Nano Research* **2019**, *12* (3), 471–487.
- (27) Gu, P.; Zhang, S.; Zhang, C.; Wang, X.; Khan, A.; Wen, T.; Hu, B.; Alsaedi, A.; Hayat, T.; Wang, X. Two-dimensional MAX-derived titanate nanostructures for efficient removal of Pb(II). *Dalton Trans.* **2019**, *48* (6), 2100–2107.
- (28) Nan, J.; Guo, X.; Xiao, J.; Li, X.; Chen, W.; Wu, W.; Liu, H.; Wang, Y.; Wu, M.; Wang, G. Nanoengineering of 2D MXene-Based Materials for Energy Storage Applications. *Small* **2021**, *17* (9), No. 1902085.
- (29) Ahmed, B.; Anjum, D. H.; Gogotsi, Y.; Alshareef, H. N. Atomic layer deposition of  $SnO_2$  on MXene for Li-ion battery anodes. *Nano Energy* **2017**, 34, 249–256.
- (30) Li, Y.; Xu, D. H.; Zhang, D. H.; Wei, Y. C.; Zhang, R. N.; Guo, Y. X. Study on MnO<sub>2</sub>/MXene-Ti<sub>3</sub>C<sub>2</sub> composite materials as cathode materials for magnesium batteries. *RSC Adv.* **2019**, 9 (58), 33572–33577.
- (31) Pazniak, H.; Plugin, I. A.; Loes, M. J.; Inerbaev, T. M.; Burmistrov, I. N.; Gorshenkov, M.; Polcak, J.; Varezhnikov, A. S.; Sommer, M.; Kuznetsov, D. V.; Bruns, M.; Fedorov, F. S.; Vorobeva, N. S.; Sinitskii, A.; Sysoev, V. V. Partially Oxidized  $\mathrm{Ti}_3\mathrm{C}_2\mathrm{T}_x$  MXenes for Fast and Selective Detection of Organic Vapors at Part-per-Million Concentrations. *ACS Applied Nano Materials* **2020**, 3 (4), 3195–3204.

- (32) He, T. T.; Liu, W.; Lv, T.; Ma, M. S.; Liu, Z. F.; Vasiliev, A.; Li, X. G. MXene/SnO<sub>2</sub> heterojunction based chemical gas sensors. *Sens. Actuators B Chem.* **2021**, 329, No. 129275.
- (33) Gasso, S.; Sohal, M. K.; Mahajan, A. MXene modulated SnO<sub>2</sub> gas sensor for ultra-responsive room-temperature detection of NO<sub>2</sub>. Sens. Actuators B Chem. **2022**, 357, No. 131427.
- (34) Yin, L.; Liu, C. G.; Ding, C. Z.; Zhao, C.; Mitrovic, I. Z.; Lim, E. G.; Wang, H. B.; Sun, Y.; Han, Y. F.; Li, Z. R.; Yang, L.; Ma, C. Q.; Zhao, C. Z. Functionalized-MXene-nanosheet-doped tin oxide enhances the electrical properties in perovskite solar cells. *Cell Rep. Phys. Sci.* **2022**, *3* (6), No. 100905.
- (35) Ding, J. F.; Tang, C.; Zhu, G. J.; Sun, W. W.; Du, A. J.; He, F. Y.; Wu, M. H.; Zhang, H. J. Integrating SnS<sub>2</sub> Quantum Dots with Nitrogen-Doped Ti<sub>3</sub>C<sub>2</sub>T<sub>x</sub> MXene Nanosheets for Robust Sodium Storage Performance. ACS Appl. Energy Mater. 2021, 4 (1), 846–854.
- (36) Zuo, D. C.; Song, S. C.; An, C. S.; Tang, L. B.; He, Z. J.; Zheng, J. C. Synthesis of sandwich-like structured Sn/SnO<sub>x</sub>@MXene composite through in-situ growth for highly reversible lithium storage. *Nano Energy* **2019**, *62*, 401–409.
- (37) Ma, Y. L.; Sheng, H. W.; Dou, W.; Su, Q.; Zhou, J. Y.; Xie, E. Q.; Lan, W. Fe<sub>2</sub>O<sub>3</sub> Nanoparticles Anchored on the Ti<sub>3</sub>C<sub>2</sub>T<sub>x</sub> MXene Paper for Flexible Supercapacitors with Ultrahigh Volumetric Capacitance. *ACS Appl. Mater. Interfaces.* **2020**, *12* (37), 41410–41418
- (38) Loes, M. J.; Bagheri, S.; Vorobeva, N. S.; Abourahma, J.; Sinitskii, A. Synergistic Effect of  $TiS_3$  and  $Ti_3C_2T_x$  MXene for Temperature-Tunable p-/n-Type Gas Sensing. ACS Applied Nano Materials 2023, 6 (11), 9226–9235.
- (39) Ding, H.; Li, Y.; Li, M.; Chen, K.; Liang, K.; Chen, G.; Lu, J.; Palisaitis, J.; Persson, P. O. A.; Eklund, P.; Hultman, L.; Du, S.; Chai, Z.; Gogotsi, Y.; Huang, Q. Chemical scissor-mediated structural editing of layered transition metal carbides. *Science* **2023**, 379 (6637), 1130–1135.
- (40) Li, Y.; Shao, H.; Lin, Z.; Lu, J.; Liu, L.; Duployer, B.; Persson, P. O. A.; Eklund, P.; Hultman, L.; Li, M.; Chen, K.; Zha, X. H.; Du, S.; Rozier, P.; Chai, Z.; Raymundo-Pinero, E.; Taberna, P. L.; Simon, P.; Huang, Q. A general Lewis acidic etching route for preparing MXenes with enhanced electrochemical performance in non-aqueous electrolyte. *Nat. Mater.* **2020**, *19* (8), 894–899.
- (41) Xu, B.; Zhu, J.; Xiao, F.; Liu, N.; Liang, Y.; Jiao, C.; Li, J.; Deng, Q.; Wu, S.; Wen, T.; Pei, S.; Wan, H.; Xiao, X.; Xia, J.; Wang, Z. Electrically Tunable MXene Nanomechanical Resonators Vibrating at Very High Frequencies. ACS Nano 2022, 16 (12), 20229–20237.
- (42) Tan, D.; Cao, X.; Huang, J.; Peng, Y.; Zeng, L.; Guo, Q.; Sun, N.; Bi, S.; Ji, R.; Jiang, C. Monolayer MXene Nanoelectromechanical Piezo-Resonators with 0.2 Zeptogram Mass Resolution. *Advanced Science* **2022**, *9* (22), No. 2201443.
- (43) Bagheri, S.; Abourahma, J.; Lu, H.; Vorobeva, N. S.; Luo, S.; Gruverman, A.; Sinitskii, A. High-yield fabrication of electromechanical devices based on suspended Ti<sub>3</sub>C<sub>2</sub>T<sub>x</sub> MXene monolayers. *Nanoscale* **2023**, *15* (3), 1248–1259.
- (44) von Treifeldt, J. E.; Firestein, K. L.; Fernando, J. F. S.; Zhang, C.; Siriwardena, D. P.; Lewis, C.-E. M.; Golberg, D. V. The effect of Ti<sub>3</sub>AlC<sub>2</sub> MAX phase synthetic history on the structure and electrochemical properties of resultant Ti<sub>3</sub>C<sub>2</sub> MXenes. *Materials & Design* **2021**, *199*, No. 109403.
- (45) Lipatov, A.; Alhabeb, M.; Lukatskaya, M. R.; Boson, A.; Gogotsi, Y.; Sinitskii, A. Effect of Synthesis on Quality, Electronic Properties and Environmental Stability of Individual Monolayer  ${\rm Ti}_3{\rm C}_2$  MXene Flakes. Advanced Electronic Materials 2016, 2 (12), No. 1600255.
- (46) Shekhirev, M.; Busa, J.; Shuck, C. E.; Torres, A.; Bagheri, S.; Sinitskii, A.; Gogotsi, Y. Ultralarge Flakes of  $\text{Ti}_3\text{C}_2\text{T}_x$  MXene via Soft Delamination. *ACS Nano* **2022**, *16*, 13695–13703.
- (47) Vorobeva, N. S.; Bagheri, S.; Torres, A.; Sinitskii, A. Negative photoresponse in  ${\rm Ti}_3{\rm C}_2{\rm T}_x$  MXene monolayers. *Nanophotonics* **2022**, 11 (17), 3953–3960.
- (48) Khaledialidusti, R.; Khazaei, M.; Khazaei, S.; Ohno, K. Highthroughput computational discovery of ternary-layered MAX phases

- and prediction of their exfoliation for formation of 2D MXenes. *Nanoscale* **2021**, *13* (15), 7294–7307.
- (49) Anayee, M.; Shuck, C. E.; Shekhirev, M.; Goad, A.; Wang, R.; Gogotsi, Y. Kinetics of  $Ti_3AlC_2$  Etching for  $Ti_3C_2T_x$  MXene Synthesis. *Chem. Mater.* **2022**, 34 (21), 9589–9600.
- (50) Alhabeb, M.; Maleski, K.; Mathis, T. S.; Sarycheva, A.; Hatter, C. B.; Uzun, S.; Levitt, A.; Gogotsi, Y. Selective Etching of Silicon from Ti<sub>3</sub>SiC<sub>2</sub> (MAX) To Obtain 2D Titanium Carbide (MXene). *Angew. Chem., Int. Ed.* **2018**, *57* (19), 5444–5448.
- (51) Natu, V.; Benchakar, M.; Canaff, C.; Habrioux, A.; Célérier, S.; Barsoum, M. W. A critical analysis of the X-ray photoelectron spectra of Ti<sub>3</sub>C<sub>2</sub>T<sub>2</sub> MXenes. *Matter* **2021**, *4* (4), 1224–1251.
- (52) Ghidiu, M.; Lukatskaya, M. R.; Zhao, M.-Q.; Gogotsi, Y.; Barsoum, M. W. Conductive two-dimensional titanium carbide 'clay' with high volumetric capacitance. *Nature* **2014**, *516*, 78.
- (53) Anasori, B.; Lukatskaya, M. R.; Gogotsi, Y. 2D metal carbides and nitrides (MXenes) for energy storage. *Nature Reviews Materials* **2017**, 2, 16098.
- (54) Bai, S.; Yang, M.; Jiang, J.; He, X.; Zou, J.; Xiong, Z.; Liao, G.; Liu, S. Recent advances of MXenes as electrocatalysts for hydrogen evolution reaction. *npj 2D Materials and Applications* **2021**, 5 (1), 78.
- (55) Kim, S. J.; Koh, H.-J.; Ren, C. E.; Kwon, O.; Maleski, K.; Cho, S.-Y.; Anasori, B.; Kim, C.-K.; Choi, Y.-K.; Kim, J.; Gogotsi, Y.; Jung, H.-T. Metallic Ti<sub>3</sub>C<sub>2</sub>T<sub>x</sub> MXene Gas Sensors with Ultrahigh Signal-to-Noise Ratio. *ACS Nano* **2018**, *12* (2), 986–993.
- (56) Shahzad, F.; Alhabeb, M.; Hatter, C. B.; Anasori, B.; Man Hong, S.; Koo, C. M.; Gogotsi, Y. Electromagnetic interference shielding with 2D transition metal carbides (MXenes). *Science* **2016**, 353 (6304), 1137–1140.
- (57) Bagheri, S.; Chilcott, R.; Luo, S.; Sinitskii, A. Bifunctional Amine- and Thiol-Modified Ti<sub>3</sub>C<sub>2</sub>T<sub>x</sub> MXene for Trace Detection of Heavy Metals. *Langmuir* **2022**, 38 (42), 12924–12934.
- (58) Petříček, V.; Dušek, M.; Palatinus, L. Crystallographic Computing System JANA2006: General features. Zeitschrift für Kristallographie Crystalline Materials 2014, 229 (5), 345–352.